Available online at www.sciencedirect.com
ScienceDirect
Geochimica et Cosmochimica Acta 70 (2006) 4770–4782
Geochimica
www.elsevier.com/locate/gca

Making continental crust through slab melting: Constraints from niobium–tantalum fractionation in UHP metamorphic rutile

Yilin Xiao [a,b,*], Weidong Sun [c,d,*], Jochen Hoefs [a], Klaus Simon [a], Zeming Zhang [e], Shuguang Li [b], Albrecht W. Hofmann [d]

[a] Geowissenschaftliches Zentrum der Universität Göttingen, Goldschmittstrasse 1, D-37077 Göttingen, Germany
[b] CAS Key Laboratory of Crust-Mantle and Environments, School of Earth and Space Sciences, University of Science and Technology of China, Hefei 230026, PR China
[c] Key Laboratory of Isotope Geochronology and Geochemistry, Guangzhou Institute of Geochemistry, Chinese Academy of Sciences, Wushan, Guangzhou 510640, PR China
[d] Max-Planck Institut f. Chemie, Postfach 3060, D-55020 Mainz, Germany
[e] Institute of Geology, Chinese Academy of Geological Sciences, Beijing 100037, PR China

Received 25 July 2005; accepted in revised form 12 July 2006

Abstract

The formation of the continental crust (CC) is one of the most important processes in the evolution of the silicate Earth. Exactly how the CC formed is the subject of ongoing debate that focuses on its subchondritic Nb/Ta ratio. Nb and Ta are "geochemical identical twins," so they usually do not fractionate from each other. Here, we show that rutile grains from hydrous rutile-bearing eclogitic layers recovered from drillcores in the Dabie-Sulu ultrahigh pressure terrain have highly variable Nb/Ta values (ranging from 5.4 to 29.1, with an average of 9.8 ± 0.6), indicating major fractionation of Nb and Ta most likely occurred during blueschist to amphibole–eclogite transformation in the absence of rutile. It is suggested that the released fluids with subchondritic Nb/Ta were transported to, and retained by, hydrous rutile-bearing eclogite in colder regions, resulting in suprachondritic Nb/Ta ratios for drier eclogite in hotter regions. Further dehydration of hydrous rutile-bearing eclogites cannot transfer the fractionated Nb/Ta values to the CC due to the low solubility of Nb and Ta in fluids in the presence of rutile, while dehydration-melting results in a major component of the CC, the tonalite–trondhjemite–granodiorite (TTG) component, which is responsible for the low Nb/Ta of the CC. Consequently, residual eclogites have variable but overall suprachondritic Nb/Ta.

1. Introduction

The formation of the Earth's continental crust (CC) is of critical importance to understand the evolution of the Earth. Currently, there are several competing models with respect to the dominant process that has shaped the major chemical feature of the continental crust. Most geologists believe melting of subducted slabs in the early history of the Earth is the major way that shaped the chemical characteristics of the CC (McDonough, 1991; Rapp and Watson, 1995; Martin, 1999; Rudnick et al., 2000; Foley et al., 2002; Rapp et al., 2003), followed by modifications (Rudnick, 1995; Gao et al., 2004), and post Archean accretions of arc-magmatism and oceanic plateaus (Abbott et al., 1997; Reynaud et al., 1999) likely through complicated processes (Collins, 2002). By contrast, Kamber et al. (2002) suggested that Archean TTG was formed in the same way as modern arc rather than slab melting as adakite. Alternatively, others proposed that melting at the bottom of the thickened oceanic crust (Smithies, 2000) was more important. How subducted slabs were melted and how the distinct chemical features of the CC were produced is, however, still a controversial topic. The debate is mainly focused on the unique subchondritic Nb/Ta value of the

* Corresponding authors. Fax: +0049 551 393982.(Y. Xiao)
E-mail addresses: yxiao@gwdg.de (Y. Xiao), weidongsun@gig.ac.cn (W. Sun).

0016-7037/$ - see front matter © 2006 Elsevier Inc. All rights reserved.
doi:10.1016/j.gca.2006.07.010

CC, and more specifically, how Nb and Ta fractionated from each other and consequently how, in detail, the CC was built (Rudnick et al., 2000; Foley et al., 2002; Rapp et al., 2003; Xiong et al., 2005).

Nb and Ta share the same valence state (+5) and have similar atomic radii for octahedral coordination (Shannon, 1976), thus behaving identically in most geochemical fractionation processes linked to the evolution of the mantle (Jochum et al., 1986, 1989; Sun and McDonough, 1989; Rudnick et al., 2000). As a result, the Nb/Ta has long been regarded as constant and chondritic (17.5) in major silicate reservoirs of the Earth (Jochum et al., 1986, 1989; Sun and McDonough, 1989), and MORB, OIB, and BABB, (e.g., Sun and McDonough, 1989; Kamber and Collerson, 2000; Sun et al., 2003), although some depleted samples may have Nb/Ta ratios considerably lower than the chondritic value (Niu and Batiza, 1997; Sun et al., 2003). In contrast, the Nb/Ta of the CC is 12–13 (Barth et al., 2000; Rudnick and Fountain, 1995), much lower than the other major silicate reservoirs of the Earth. Therefore, the negative Nb and Ta anomalies and subchondritic Nb/Ta values are among the most distinct features of the CC (Taylor and McLennan, 1985; Rudnick and Fountain, 1995; Plank and Langmuir, 1998; Barth et al., 2000), and are of critical importance for understanding the formation of the CC (McDonough, 1991; Foley et al., 2002; Rudnick et al., 2000; Rapp et al., 2003).

In the last decade, analytical techniques for Nb and Ta have been improved considerably, represented by laser ablation-ICP-MS, which solves the problems of incomplete dissolution of accessory minerals that host Nb and Ta and of memory-effects in solution ICP-MS particularly for samples with high Ta concentration. The precision of Nb/Ta for laser ablation-ICP-MS data can be as good as 2%, whereas the accuracy depends heavily on the external standards used. Nonetheless, the Nb/Ta of NIST610 glass is reasonably well confined (Sun, 2003). Isotope dilution method has also been applied to Ta analyses, which have revealed large variations in Nb/Ta (Munker et al., 2003; Weyer et al., 2003). Based on data obtained using isotope dilution method, a new chondritic Nb/Ta of 19.9 ± 0.6 has been suggested; meanwhile, Nb/Ta of 14.0 ± 0.3 has been suggested for the primitive mantle, using a correlation between Zr/Hf and Nb/Ta, assuming a chondritic Zr/Hf value in the primitive mantle (Munker et al., 2003). Considering all factors together, in this paper we take Nb/Ta = 17.5 as the chondritic value and as the value for the primitive mantle (McDonough and Sun, 1995).

Given that rutile is the dominant carrier of Nb and Ta (Foley et al., 2000; Schmidt et al., 2004; Klemme et al., 2005; Xiong et al., 2005) and a common minor phase in high-grade metamorphic rocks (Chopin et al., 1991; Carswell et al., 1996; Gao et al., 1999; Liou et al., 1998; Tsujimori, 2002; Zack et al., 2002; Spandler et al., 2003), rutile has long been regarded as the controlling factor that resulted in Nb, Ta depletion in the continental crust, while the subchondritic Nb/Ta of the CC has been attributed to the melting of subducted slabs in the presence of rutile (Rudnick et al., 2000; McDonough, 1991), probably in garnet amphibolite or eclogite facies (Rapp and Watson, 1995; Rapp et al., 2003). This model has been challenged by partitioning data, which indicate that rutile favors Ta over Nb (Foley et al., 2002; Schmidt et al., 2004; Klemme et al., 2005; Xiong et al., 2005), such that partial melting of rutile-bearing eclogites with chondritic Nb/Ta results in suprachondritic Nb/Ta in the melts (Foley et al., 2002). Considering that Nb is more compatible than Ta in amphibole, a low degree of partial melting of subducted oceanic crust in the form of amphibolite was proposed (Foley et al., 2002), which, however, was questioned by Rapp et al. (2003) due to the difficulty to plausibly explain other major and trace element features of the CC. Therefore, the subchondritic Nb/Ta ratio of the CC was interpreted as the result of melting of hydrous rutile-bearing eclogitic sources with initially low Nb/Ta ratios (Rapp et al., 2003; Xiong et al., 2005), e.g., arc crust and special basalts from seamounts (Rapp et al., 2003). Nevertheless, the arc crust is not likely to be a major source of TTG, while basalts with low Nb/Ta ratios are rare and usually very depleted in incompatible elements (Niu and Batiza, 1997). Therefore, none of these models can account for all the Nb and Ta features of the continental crust. Here, we report highly variable but overall subchondritic Nb/Ta ratios in eclogitic rutile, indicating major Nb, Ta fractionation in subducted slabs that can conceivably reconcile different lines of observations.

2. Geological background and samples

As the largest ultrahigh-pressure (UHP) metamorphic terrain so far found worldwide, the Dabie-Sulu orogenic belt, which represents a Triassic collision zone between the North China Block and Yangtze Block, has attracted extensive interest from the geoscience community (Li et al., 1993, 1994, 2000; Liou and Zhang, 1995; Zhang et al., 1995, 1998, 2003, 2005; Carswell et al., 2000; Liou et al., 2000; Yang and Jahn, 2000; Sun et al., 2002). Research activities over the past decade have documented a number of characteristic features of this area, including rapid subduction to depths of greater than 100 km followed by rapid initial uplift (Xu et al., 1992; Li et al., 1993), the abundance of hydroxyl-bearing UHP mineral phases (Okay, 1995; Zhang et al., 1995), interaction between meteoric water and the rocks (Yui et al., 1995; Zheng et al., 1998), and variable fluid phases during UHP metamorphism (Xiao et al., 2000; Fu et al., 2001; Xiao et al., 2002).

The Chinese Continental Scientific Drilling Program (CCSD) in the southern limb of the Su–Lu ultrahigh-pressure metamorphic terrain in eastern China aims to reconstruct the formation and exhumation mechanisms of UHP terrains. The project consists of three pilot holes and a 5000 m main hole (Xu, 2004). ZK 703 is one of the pilot holes and about 70 m away from the main hole, with a depth of 558 m and a core-recovery >85%. The

penetrated rocks consist mainly of a rutile-rich eclogitic layer with a composite thickness of about 300 m, which is interlayered by gneiss, phengite–quartz schist, jadeite quartzite and kyanite quartzite (Fig. 1). Geological survey indicates that this layer covers an area of about $3500 \times 200\ m^2$ (Xu et al., 1998). Rutile occurs in all eclogites with volume percents of 1–5%. Coesite relics as inclusions in garnet and omphacite suggest that the eclogitic layer has been subducted to depths >100 km and subjected to peak metamorphic temperatures of 700–880 °C (Zhang et al., 2004).

Investigated samples were collected from the rutile-rich eclogitic layer of ZK 703, including an eclogitic sample and a nearby quartz vein sample. The eclogitic sample (703-27a) consists mainly of garnet, omphacite, albite + amphibole symplectite, and coarse-grained rutile (~5 vol %, some grains are up to 6 mm in size). Petrological observations indicate that the assemblage of coarse-grained garnet + omphacite + rutile represents the peak of an early eclogite-facies metamorphic stage. Most garnet grains are relatively large, ranging from 1 to 2 mm. As shown in Table 1, garnet is compositionally homogeneous, and is rich in almandine and grossular (~49 and ~30 mol %, respectively), with low pyrope (<20 mol %) and minor spessartine (around 1 mol %). Omphacite occurs either in the matrix or as inclusions in garnet, with jadeite contents up to 58 mol %. During retrograde metamorphism from eclogite- to amphibolite- and/or greenschist-facies, the eclogite-facies minerals were partially or totally replaced by symplectitic mineral coronas. Retrograde reactions include the formation of amphibole coronas around garnet, replacement of omphacite by symplectite of amphibole + plagioclase + clinopyroxene. The nearby quartz vein sample (703-27b) is composed of quartz and coarse-grained rutile (up to 8 mm in size). Quartz–garnet and quartz–rutile oxygen isotopic thermometers suggest peak metamorphic temperatures of 830 and 620 °C for the eclogite and the vein samples, respectively (Xiao, unpublished data).

Rutile in both samples occurs as euhedual to subhedral grains, up to 2–8 mm in diameter. The five rutile grains selected for analyses are 6–8 mm in size. Thin titanite replacement (10–20 μm) surrounding coarse-grained rutile in the eclogitic sample indicates only very limited retrogression for rutile (Fig. 2A). Coarse-grained rutiles in the quartz vein show even less retrogression compared to those in the eclogitic sample, with only a thin ilmenite rim (of a few μm) at the margin (Fig. 2B).

3. Analytical method

All analyses have been carried out at the Geoscience Centre, University of Göttingen. Whole rock major elements of the eclogitic sample were determined by X-ray fluorescence (XRF) on glass discs using a Philips PW 1480 automated sequential spectrometer (see Hartmann, 1994). It has to be noted that, because of the scarcity of sample material, the analyzed sample 703-27a (see Table 1) with less than 50 g, does not include the investigated coarse-grained rutiles. Therefore, the "whole rock" value is not representative for the trace element content of rutile, especially when discussing their Nb and Ta characteristics as these two elements are mainly controlled by rutile.

Minerals analyses were completed using a JXA-8900RL JEOL Superprobe equipped with wavelength-dis-

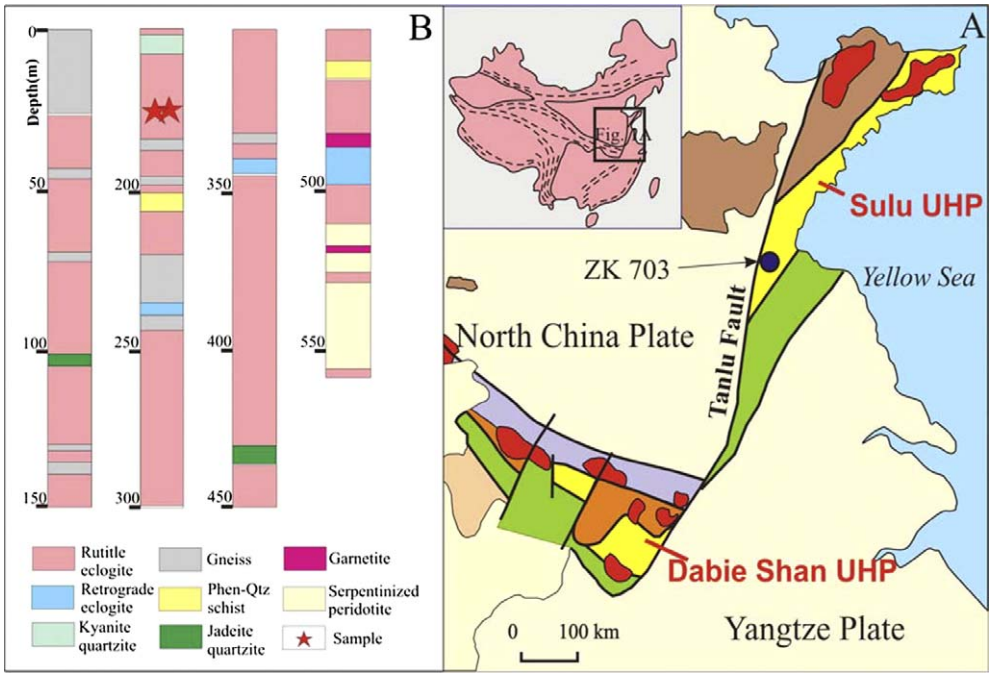

Fig. 1. (A) Simplified geological map of the Dabie-Sulu orogenic belt showing major geological features of the Dabie-Sulu UHP metamorphic belt and the location of the CCSD drill site. (B) Simplified lithological profile of ZK703.

Table 1
Representative mineral and whole rock compositions of the investigated eclogite

	Grt (rim)	Grt (core)	Cpx (rim)	Cpx (core)	Cpx (in)[a]	Pl	Am (sym) [a]	Am (grt)[a]	Am (rut)[a]		Whole rock[b]
SiO_2	38.9	38.7	56.6	56.8	57.0	66.9	40.2	41.8	42.4		43.2
TiO_2	0.062	0.091	0.068	0.074	0.076	0.016	0.533	0.137	0.609		4.49
Al_2O_3	21.5	21.4	13.5	13.5	13.6	20.4	14.5	16.8	15.5		14.9
Cr_2O_3	0.017	0.015	0.028	0.017	0.019	0.012	0.000	0.000	0.018		0.010
FeO[c]	23.4	23.5	4.00	4.01	4.31	0.25	14.9	16.1	14.4		16.5
MnO	0.563	0.669	0.000	0.017	0.060	0.017	0.155	0.107	0.238		0.34
MgO	5.21	5.07	6.19	6.27	6.14	0.02	11.10	8.09	9.71		5.83
CaO	10.7	10.7	9.92	9.87	9.93	0.69	10.0	8.09	8.87		9.69
Na_2O	0.025	0.026	8.62	8.72	8.84	11.5	3.88	5.04	4.45		2.93
K_2O	bd	bd	bd	bd	bd	0.09	1.19	0.32	0.85		0.010
										P_2O_5	0.873
Total	100	100	98.9	99.2	100	99.8	96.4	96.5	97.0		98.8
Si	3.00	2.99	2.01	2.01	2.01	2.93 T-site				V (ppm)	161
Ti	0.004	0.005	0.002	0.002	0.002	0.001 Si	6.02	6.22	6.28	Co	19.2
Al	1.96	1.96	0.57	0.56	0.56	1.05 Al(4)	1.98	1.78	1.72	Ni	14.9
Cr	0.001	0.001	0.001	0.0005	0.001	0.0004 M(123)				Y	71.5
Fe^{3+}	0.029	0.048	0.000	0.008	0.022	0.009 Ti	0.060	0.015	0.068	Zr	244
Fe^{2+}	1.48	1.47	0.119	0.111	0.105	0.000 Al(6)	0.576	1.17	0.977	Nb	9.20
Mn	0.037	0.044	0.000	0.001	0.002	0.001 Cr	0.000	0.000	0.002	La	9.33
Mg	0.600	0.585	0.328	0.331	0.322	0.001 Fe^{3+}	0.705	0.479	0.352	Ce	18.7
Ca	0.886	0.890	0.378	0.375	0.374	0.032 Mg	2.48	1.80	2.14	Nd	12.9
Na	0.004	0.004	0.594	0.599	0.603	0.972 Mn	0.020	0.013	0.030	Sm	5.04
K	bd	bd	bd	bd	bd	0.005 Fe^{2+}	1.16	1.53	1.43	Lu	0.966
Total	8.00	8.00	4.00	4.00	4.00	5.00 M(4)				Hf	5.17
						Ca	1.61	1.29	1.41	Ta	0.644
Prp	0.200	0.196 Jd	0.582	0.577	0.578 Ab	0.963 Na (M4)	0.390	0.709	0.592	W	11.1
Grs	0.295	0.297 Ac	0.000	0.008	0.022 An	0.032 A-site				Pb	4.94
Alm	0.493	0.492 Di	0.285	0.288	0.289 Or	0.005 Na (A)	0.738	0.746	0.686	Th	0.746
Spe	0.012	0.015 Hed	0.103	0.096	0.094	K	0.227	0.060	0.161	U	0.237

[a] Cpx (in), omphacite inclusion in garnet; Am (Sym), amphibole occurring in symplectite; Am (grt) and Am (rut), amphiboles around garnet and rutile, resepctively.
[b] Major elements of whole-rock (703-27a) were determined by XRF, whereas trace elements were analyzed using laser-ICP-MS on the same XRF glass disc.
[c] Total Fe as FeO.

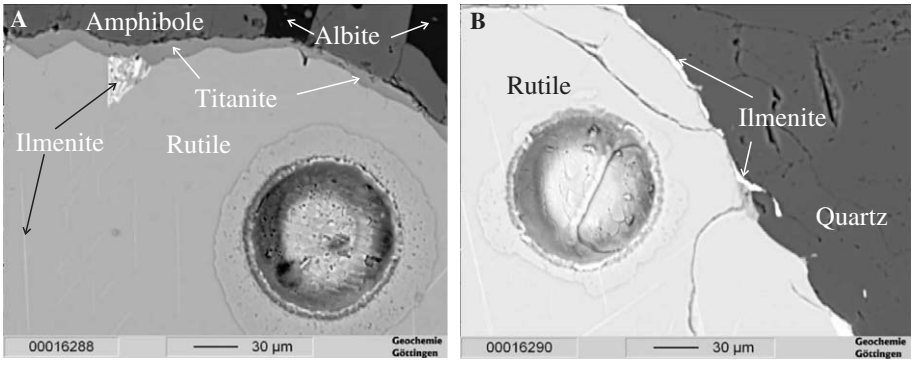

Fig. 2. Back-scattered electron scanning images of coarse-grained rutiles in the investigated samples. The holes represent laser ablation-ICP-MS spots. Note there is only very thin titanite replacement (10–20 µm) surrounding coarse-grained rutile in the eclogitic sample (A), whereas coarse-grained rutile in the quartz vein shows a thin ilmenite rim (a few µm) at the margin (B).

persive spectrometers (WDS) and energy dispersive spectrometer (EDS) combined micro-analyzer. Operating conditions were 15.0 kV accelerating voltage, 15 nA beam current and 10 µm electron beam diameter. Standards included silicates and pure oxides (see Xiao et al., 2005 for details).

Nb, Ta, and other trace elements of rutile were analyzed by laser ablation (LA) ICP-MS using an ArF-Excimer laser

source "Compex 110" ($\lambda = 193$ nm; repetition rate of 10 Hz) coupled to a Perkin-Elmer DRC II ICP-MS. All samples have been prepared as polished thin sections (ca. 200 μm thick). ^{49}Ti was used as an internal standard; NIST 610 was used as a calibration standard. Reproducibility and accuracy of trace element concentrations were assessed to be better than 10%. Ablation spots were around 80 μm, with the laser energy of ~200 mJ. The ablated aerosol was carried to the ICP source with Ar gas.

To check for systematic shifts of measured Nb and Ta concentrations and Nb/Ta ratios, we measured a few MPI-DING glasses (Atho-g1, KL2-g, StHs6/80) (Jochum et al., 2000) and a pure rutile crystal (R10 from T. Zack, Heidelberg) with Ti-content ranging from 0.147 to 60 wt%. Obtained ratios show little systematic dependence on increasing Ti-content (Table 2 and Fig. 4): a positive deviation of <5% for MPI-DING glasses (mostly <3%) when compared to well calibrated values of (Jochum et al., 2000), and ~9% for pure rutile (R10) when compared to Zack's data (unpublished) that have been measured at the Mineralogisches Institut in Heidelberg. Our LA-ICPMS measurements gave a mean Nb/Ta value of 6.2 ± 0.1 ($2\sigma = 1.4\%$) calculated from three repeated measurements for R10, close to the average value of 5.6 ± 0.3 given by Zack (unpublished data).

After "in situ" LA-ICP-MS measurements, thin sections have been re-polished and analyzed by electron microprobe. All analyzed spots have been qualitatively checked by electron microprobe in order to ensure that LA-ICP-MS measurements were done on rutile rather than on retrograde ilmenite or titanite. Furthermore, Nb, Ta and other trace element concentrations of 49 selected LA-ICP-MS spots were conducted with the JXA-8900RL JEOL Superprobe, with the purpose to rule out any Nb and Ta fractionations due to laser ablation and electron bombardment (Table 3). Analyses were performed at 25 kV acceleration voltage, 80 nA beam current and 8 μm probe diameter. Peak counting and background counting were, respectively, set at 15 and 10 s for Ti, 150 and 100 s for Si, Al, and Fe, 200 and 200 s for V, Cr, Sn, and 300 and 300 s for Nb, Ta, and Zr, taking altogether ca. 21 min for each analysis. Every 10 analyses were bracketed by a synthetic rutile standard for zero-concentration count rates on the peaks and to exclude any machine drift (Zack et al., 2004). Detection limits were calculated to be 30 ppm for Cr and Al, 40 ppm for Fe, V and Zr, 60 ppm for Ta and Sn, 70 ppm for Nb and Si, and 1400 ppm for Ti (2σ).

4. Fractionated Nb/Ta in rutile

Rim-core-rim analyses were carried out on five rutile grains ranging from 5 to 8 mm in size. To reveal two-dimensional inhomogeneities of Nb and Ta in rutile, more analyses on the core (c), the mantle (m) and the rim (r) of two rutile grains were carried out besides the profile analysis (Fig. 3) . The Nb and Ta contents range from 338 to 2800, 23.8–248 ppm, respectively, with Nb/Ta values ranging from 5.40 to 29.1 (Table 3). Compared to the eclogitic sample, rutile grains in the quartz vein usually have higher Nb and Ta contents. Remarkably, although concentrations of Nb and Ta measured by electron microprobe are 20–30% lower than those from the LA-ICP-MS, both methods indicate that rutile grains have subchondritic Nb/Ta ratios with high Nb, Ta contents in the cores, which change sharply to suprachondritic Nb/Ta ratios with lower Nb, Ta contents near the rims, forming "Nb/Ta spikes." In a few cases, the Nb/Ta decreases and the Nb, Ta contents increase further to the rims (Fig. 5). Such abrupt variations cannot be explained by a closed system; instead, the results suggest that rutile has collected Nb and Ta from at least

Table 2
Comparison between measured and reference values of various standards

	Ti	V	Zr	Nb	Hf	Ta	W	Pb	Th	U	Nb/Ta
atho-g1	1470	3.50	675	70.0	18.3	4.19	12.3	5.59	10.5	3.35	16.7
Ref. value[a]	1470	4.40	524	61.9	13.6	3.81		5.70	7.48	2.35	16.2
KL2-g-1	15600	420	215	16.9	5.70	1.08	1.07	2.63	1.46	1.10	15.6
KL2-g-2	15600	416	218	16.9	5.69	1.07	0.599	2.39	1.47	0.851	15.8
Ref. value[a]	15600	370	159	15.8	4.14	0.970	0.400	2.20	1.03	0.550	16.3
StHs6/80-G	4100	115	176	7.63	4.46	0.461	0.085	9.67	3.22	0.87	16.6
Ref. Value[a]	4100	96.0	120	7.10	3.16	0.418		10.2	2.22	1.03	17.0
ML3B-G-1	12500	373	174	9.45	4.47	0.608	0.533	1.77	0.776	0.654	15.5
ML3B-G-2	12500	374	175	9.52	4.60	0.595	0.518	1.76	0.820	0.659	16.0
Ref. value[a]	12500		126	9.00	3.32	0.550		1.45	0.540	0.440	16.4
R10.1 (core)	600000	1350	1100	2970	53.9	476	124	0.575	0.007	63.4	6.24
R10.2 (middle)	600000	1361	1060	3070	51.7	502	128	0.041	0.022	64.7	6.12
Ref. value[b]	600000		788	2730	38.9	504					5.42
R10.3 (rim)	600000	1700	943	2870	45.3	460	95.1	0.352	0.097	51.5	6.24
Ref. value[b]	600000		769	2590	37.4	456					5.68

[a] Published values by Jochum et al. (2000).
[b] Values from Thomas Zack (unpublished data).

Table 3
Nb, Ta, and other trace element concentrations in rutile grains from drilling hole in eastern China

	Ti[a]	V	Zr	Nb	Hf	Ta	W	Th	U	Nb/Ta	V[b]	Zr[b]	Nb[b]	Ta[b]
Grain 27a-1														
−1	599000	1380	228	727	9.01	130	22.1	0.023	1.47	5.59	936	141	512	n.d.
−2	600000	1200	196	991	7.60	57.9	20.2	n.d.	1.09	17.1	969	138	997	n.d.
−3	601000	1160	194	1250	6.93	127	17.5	0.004	1.18	9.90	963	155	1070	87.6
−4	599000	1160	196	1020	6.87	84.2	18.3	0.020	2.07	12.1	941	155	884	50.8
−5	599000	1420	227	1330	9.44	125	24.7	0.071	1.30	10.7	932	122	877	80.3
−6	601000	1190	184	1220	6.96	145	17.4	0.083	1.51	8.38	922	126	1050	116
−7	597000	1230	179	1510	7.82	143	24.2	0.020	1.49	10.6	1060	144	1220	112
−8	596000	1180	171	1320	6.51	155	18.4	0.005	0.86	8.50	1230	120	1260	133
−9	596000	1180	180	1410	6.71	155	31.7	0.037	1.22	9.08	1130	149	1100	148
−10	591000	1160	176	1360	6.78	149	24.7	0.006	0.79	9.12	1130	146	1000	55.7
−11	600000	1250	174	1320	5.78	138	18.0	0.016	1.11	9.58	990	100	1090	172
−12	597000	1180	188	1520	7.31	157	20.3	0.014	1.26	9.68	997	127	1170	197
−13	586000	1210	181	1330	6.85	162	23.6	n.d.	0.85	8.23	1180	134	905	179
−14	593000	1110	188	429	7.68	24.0	15.8	0.004	0.64	17.8	1110	144	317	n.d.
−15	594000	1130	178	531	7.11	27.6	23.6	n.d.	0.64	19.2	1080	170	449	n.d.
−16	601000	1120	185	678	6.96	46.5	17.5	0.017	1.17	14.6	971	130	505	n.d.
Grain 27a-2														
−1	600000	1380	218	1000	8.87	125	20.1	0.081	1.48	8.03				
−2	600000	1230	187	2200	9.08	248	36.3	0.005	1.08	8.88				
−3	600000	1090	164	1180	7.19	161	16.2	0.034	1.02	7.35				
−4	600000	1070	171	909	7.72	62.1	14.7	0.045	1.18	14.6				
−5	600000	1130	190	1900	7.81	179	26.8	n.d.	3.38	10.6				
−6	599000	1120	195	2060	8.41	182	41.4	n.d.	3.15	11.3		175	1860	155
−7	600000	1100	198	1450	7.76	180	29.0	n.d.	3.17	8.04				
−8	597000	1090	189	1390	6.93	144	22.8	0.008	2.22	9.64		195	1470	161
−9	600000	1120	193	1740	8.99	169	47.4	0.022	3.00	10.3				
−10	600000	1130	201	1680	9.45	160	40.9	0.008	3.69	10.5				
−11	600000	1100	215	1550	8.62	181	42.8	0.022	3.87	8.53				
−12	600000	1070	200	1100	8.33	69.8	46.2	n.d.	2.84	15.7				
−13	600000	1210	189	1440	8.58	170	45.7	0.009	3.53	8.44				
−14	596000	1050	176	590	8.33	40.1	33.8	0.009	1.29	14.7	1110	147	452	60.6
c1	599000	1080	193	1370	8.27	132	27.5	0.007	5.59	10.3			1110	128
c2	600000	1080	196	1220	9.14	128	17.9	0.008	4.93	9.50				
c3	598000	1110	182	1590	7.64	191	24.4	n.d.	2.78	8.34			1370	170
c4	600000	1080	185	1960	7.48	172	42.8	0.006	2.40	11.4				
c5	600000	1090	180	1450	6.50	116	29.7	0.008	1.56	12.5				
m1	598000	1110	197	1860	8.35	172	46.4	0.007	4.74	10.8			1470	86.8
m2	600000	1060	168	774	7.96	70.2	15.4	n.d.	2.42	11.0				
m3	600000	1150	181	2800	8.47	240	63.5	n.d.	1.43	11.7				
m4	600000	1030	174	861	8.44	103	16.7	0.022	1.28	8.34				
m5	600000	1040	174	951	6.58	172	18.8	n.d.	1.36	5.52				
m6	600000	1070	173	739	7.25	58.1	13.7	n.d.	2.18	12.7				
m7	596000	1080	172	1220	6.89	137	18.9	n.d.	3.59	8.93			1060	114
m8	600000	1120	174	1580	6.95	152	34.1	0.029	2.15	10.4				
m9	600000	1100	182	1510	8.17	153	35.2	0.005	2.33	9.88				
r1	600000	1060	164	604	6.16	42.5	20.8	n.d.	1.66	14.2				
r2	599000	1070	171	596	7.18	42.7	21.5	n.d.	4.31	14.0	951	137	514	n.d.
r3	600000	1090	154	995	5.78	149.8	19.1	0.009	1.86	6.64				
r4	600000	1090	165	685	7.10	127.3	13.5	n.d.	1.22	5.38				
r5	600000	1020	159	460	6.53	35.0	15.4	0.010	0.980	13.1				
r6	600000	1050	154	750	5.38	102	13.5	0.009	0.878	7.39				
r7	597000	1090	161	1540	7.96	175	38.2	n.d.	1.12	8.81	978	151	1190	188
r8	597000	1110	180	1560	7.86	181	29.2	n.d.	1.37	8.63	959	140	1170	58.1
r9	600000	1030	175	366	7.79	29.6	12.7	0.019	1.13	12.4				
r10	600000	1040	159	391	6.37	30.1	15.5	0.018	1.52	13.0				
r11	600000	1030	164	417	7.19	35.4	22.5	0.348	2.10	11.8				
r12	600000	1050	159	338	6.78	23.8	13.2	n.d.	1.50	14.2				
r13	600000	1030	138	409	5.72	31.5	13.5	0.008	1.06	13.0				
r14	600000	1030	164	362	5.98	23.9	13.3	0.008	1.30	15.1				
r15	600000	1060	170	929	6.31	118	32.7	n.d.	1.15	7.85				

(*continued on next page*)

Table 3 (*continued*)

	Ti[a]	V	Zr	Nb	Hf	Ta	W	Th	U	Nb/Ta	V[b]	Zr[b]	Nb[b]	Ta[b]
Grain 27b-1														
−1	600000	1090	325	1180	11.7	150	32.4	0.651	4.52	7.89				
2	600000	1110	477	1480	14.8	135	39.3	1.19	6.57	10.9				
3	600000	1160	431	1500	15.4	134	44.1	0.898	6.80	11.2				
4	600000	1440	311	1510	86.3	129	65.8	9.38	15.1	11.7				
5	600000	1160	198	1520	9.88	155	45.3	0.009	9.12	9.81				
6	600000	1150	194	1500	8.02	157	48.7	0.041	9.31	9.53				
7	600000	1110	199	1490	8.12	156	48.2	0.023	9.51	9.58				
8	600000	1190	209	1590	9.00	158	49.4	0.010	8.60	10.1				
9	600000	1190	209	1590	10.1	161	45.9	0.012	9.53	9.89				
10	600000	1110	197	1570	8.49	147	51.2	0.010	10.9	10.6				
11	600000	1160	209	1710	9.28	193	55.4	n.d	8.23	8.87				
12	600000	1160	205	1740	9.60	201	65.6	0.061	9.58	8.63				
14	600000	1150	195	1700	8.64	184	58.9	n.d	6.56	9.21				
15	600000	1120	201	1560	9.82	124	49.1	0.010	5.71	12.6				
16	600000	1160	199	1600	8.46	137	50.5	0.028	5.36	11.7				
17	600000	1140	194	1260	8.49	129	42.4	0.054	5.51	9.78				
18	600000	1050	193	660	6.52	34.4	31.8	n.d.	4.74	19.2				
rim1	600000	1480	253	1800	9.77	208	53.9	0.023	5.88	8.66				
rim2	600000	1090	186	830	9.32	28.6	22.9	0.012	4.74	29.1				
Grain 27b-2														
−1	600000	1070	189	1080	7.06	147	34.1	n.d.	3.88	7.38	1010	148	883	90.1
−2	599000	1120	199	1570	9.79	143	40.3	n.d.	5.57	11.0	1010	170	1430	60.6
−3	598000	1170	208	1590	9.52	144	45.7	0.006	6.38	11.0	1020	177	1430	102
−4	595000	1210	212	1650	8.61	145	48.7	0.007	6.79	11.4	1020	161	1380	148
−5	598000	1130	210	1570	9.66	150	46.6	0.016	6.45	10.5	976	176	1440	128
−6	597000	1120	209	1560	9.17	148	45.3	0.007	8.26	10.5	1010	157	1370	148
−7	593000	1150	214	1580	8.80	149	44.5	0.015	7.43	10.6	1110	189	1420	181
−8	598000	1130	214	1570	8.55	150	41.6	n.d.	7.43	10.4	950	178	1360	164
−9	598000	1120	215	1590	8.48	150	43.1	0.046	7.63	10.6	1040	145	1380	91.7
−10	598000	1110	218	1580	8.91	156	43.0	n.d.	8.03	10.1	1050	165	1430	98.3
−11	600000	1120	197	1290	6.79	148	32.3	n.d.	4.38	8.73	989	153	935	154
Grain 27b-3														
−1	598000	1360	212	1630	9.98	184	45.0	0.010	8.93	8.85	941	150	827	72.1
−2	600000	1350	220	1780	9.98	167	46.5	n.d.	6.32	10.6	932	168	1600	138
−3	599000	1350	228	1800	10.7	187	50.5	0.009	6.75	9.61	1010	162	1590	143
−4	600000	1350	229	1750	10.2	185	53.1	n.d.	8.27	9.43	969	167	1530	155
−5	594000	1350	237	1730	11.5	180	52.8	n.d.	8.38	9.61	982	180	1530	179
−6	597000	1340	236	1690	11.0	169	49.8	0.008	8.88	10.0	963	193	1490	175
−7	600000	1350	237	1770	11.5	170	54.1	n.d.	9.56	10.4	978	184	1410	102
−8	599000	1340	240	1860	9.94	213	62.4	0.011	8.32	8.73	1000	183	1380	115
−9	598000	1360	226	1840	10.9	235	69.0	n.d.	8.45	7.84	978	146	1460	176
−10	599000	1330	224	1850	8.82	225	69.0	0.008	7.44	8.20	971	160	1430	159
−11	597000	1350	221	1880	10.4	223	67.6	0.030	6.50	8.43	990	173	1410	80.3
−12	600000	1290	207	1150	8.91	114	43.4	n.d.	4.61	10.0	995	181	1000	86.8
c1	600000	1400	227	1920	10.0	176	55.3	0.008	7.55	10.9				
c2	600000	1390	240	2080	10.1	219	64.4	n.d.	7.27	9.50				
c3	600000	1340	230	1800	9.74	169	54.6	n.d.	8.21	10.7				
c4	600000	1370	241	1830	10.3	173	52.4	n.d.	9.60	10.6				
c5	600000	1410	213	1840	9.35	165	50.5	n.d.	5.76	11.2				
c6	600000	1350	231	1880	10.1	168	51.5	n.d.	8.09	11.2				
m1	600000	1370	233	1880	10.7	200	54.2	n.d.	5.89	9.42				
m2	600000	1380	224	1850	10.7	157	55.5	n.d.	5.10	11.8				
m3	600000	1370	229	1810	10.0	168	50.3	0.008	8.15	10.8				
m4	600000	1340	232	1850	8.88	173	52.2	0.010	6.53	10.7				
m5	600000	1340	220	1770	9.46	183	52.1	0.026	5.34	9.66				
m6	600000	1370	212	1740	8.53	148	43.5	0.019	7.37	11.7				
m7	600000	1360	229	1810	9.47	161	47.1	n.d.	8.34	11.2				
m8	600000	1350	231	1880	9.32	172	46.4	0.010	4.98	10.9				
r1	600000	1310	195	1210	9.34	149	35.7	0.059	4.86	8.08				
r2	600000	1310	206	1480	9.85	174	43.7	0.046	4.39	8.53				
r3	600000	1310	182	1300	7.66	172	26.7	n.d.	3.43	7.53				
r4	600000	1320	221	1200	9.10	80.5	57.3	n.d.	6.21	14.9				
r5	600000	1260	216	745	7.30	44.1	24.1	0.010	5.21	16.9				
r6	600000	1340	208	1110	9.05	149	32.5	0.062	4.50	7.41				

Table 3 (*continued*)

	Ti[a]	V	Zr	Nb	Hf	Ta	W	Th	U	Nb/Ta	V[b]	Zr[b]	Nb[b]	Ta[b]
r7	600000	1320	212	1100	8.87	178	34.8	0.010	3.69	6.17				
r8	600000	1320	206	1420	8.06	168	38.6	n.d.	4.83	8.46				
r9	600000	1360	211	1480	8.79	170	36.6	0.010	4.97	8.75				
r10	600000	1300	243	1510	7.94	178	40.3	0.010	4.84	8.50				
r11	600000	1330	213	1340	8.41	151	39.3	n.d.	4.27	8.92				
r12	600000	1330	218	1400	9.61	169	30.8	n.d.	4.47	8.30				
r13	600000	1360	221	1840	8.46	202	50.6	n.d.	3.44	9.12				
r14	600000	1300	211	1220	9.74	120	44.5	0.022	3.33	10.2				

Five rutile grains were analyzed: 27a-1 and 27a-2 are from the eclogitic sample, whereas 27b-1, 27b-2, and 27b-3 are from the nearby quartz vein. Continuous numbers (1, 2, 3...) indicate rim-core-rim profile analyses; whereas analytical spots starting with c, m, r represent the geographic core, the middle zone, and the rim of the grain, respectively.

n.d. not detected.

[a] A minor isotope of Ti (^{49}Ti) was used as an internal standard, assuming that Ti content in rutile is 60 wt% when not measured.

[b] Values measured by electron microprobe.

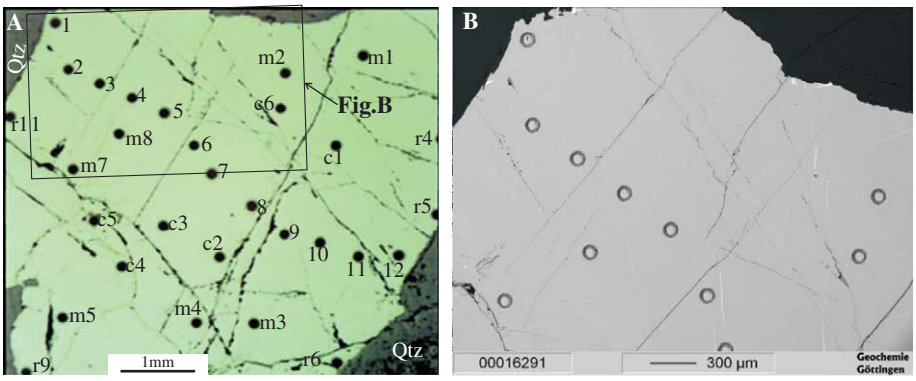

Fig. 3. Photomicrographs of an investigated rutile (grain 27b3), showing that all analyzed points are rutile rather than ilmenite or titanite. Continuous numbers (1, 2, 3...) indicate rim-core-rim analyses; whereas analytical spots starting with c, m, and r represent the geographic core, middle zone, and rim of the grain, respectively.

two sources—first a subchondritic source, then a suprachondritic one, and in some cases, finally back to the subchondritic source. Consistently, the Nb/Ta spikes are also separated in Nb/Ta versus Nb and U diagrams, with systematically lower U and Nb (Fig. 6). All these features indicate that both Nb and Ta were mobile. Nonetheless, the average Nb/Ta of all the analyses weighted by Nb, Ta contents is 9.8 ± 0.6, which is much lower than the chondritic value (17.5) (McDonough and Sun, 1995), and also lower than that of Dabie eclogites sampled from the surface (Sun, unpublished data) and their protoliths, and Neoproterozoic mafic dykes in south China (Li et al., 2002), indicating significant Nb, Ta fractionation. Remarkably, the average Nb/Ta ratio of ~10 is even lower than the Nb/Ta values of the CC (12–13) (Barth et al., 2000).

It is worth to consider whether the high Nb/Ta spikes observed in the present study are just mineral-scale features, reflecting prograde mineral breakdown reactions, or alternatively, reflecting the characteristics of "zone refining" dehydrations. So far, to our knowledge, no mechanism is known that can fractionate Nb/Ta by a factor of 2 on the mineral-scale of rutile. Therefore, we consider that the high Nb/Ta spikes can be better explained by a "zone refining" dehydration model (see below).

5. Discussion and conclusion

5.1. Mobility and fractionation of Nb and Ta

The highly variable Nb/Ta ratios in the studied rutile indicate major fractionation between the two elements in the subducted slab. Moreover, the presence of thick rutile-rich layers suggests that Ti is mobile during subduction. These observations are remarkable because Nb, Ta and Ti are all regarded as conservative elements that are not mobile during subduction as indicated by arc magmas (Pearce and Peate, 1995).

It has been experimentally shown that Nb and Ta are highly soluble in fluids in the absence of rutile (Stalder et al., 1998), and that Nb and Ta are immobile in the presence of rutile (e.g., Brenan et al., 1994). Low Nb/Ta ratios found by Henry et al. (1996) in a rutile bearing eclogitic vein compared to its wall rocks was taken as an indicator of Nb and Ta mobility in the presence of rutile. However, in our view, these low ratios can be better explained by the hypothesis that Nb and Ta were mobile before rutile appears, and then were retained by newly formed rutile under suitable pressures and temperatures. We propose that the Nb/Ta fractionation and the mobility of Ti are probably

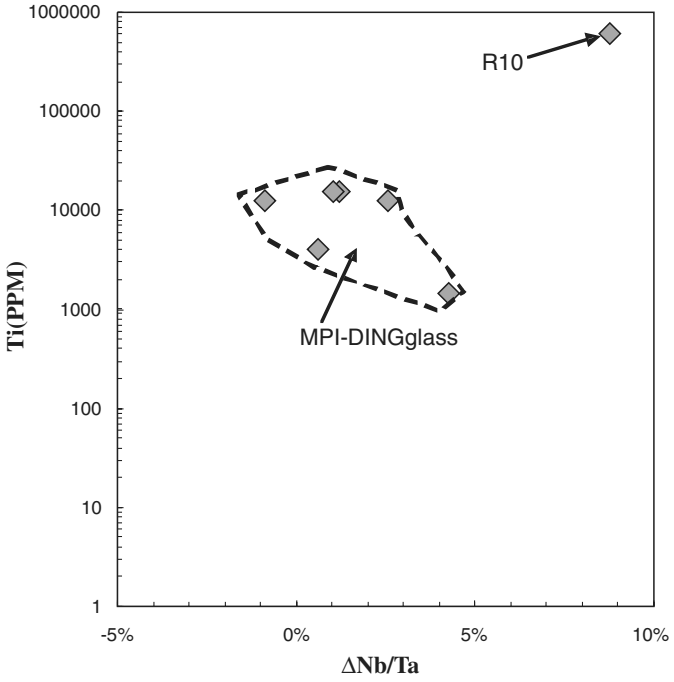

Fig. 4. Ti vs. $\Delta_{Nb/Ta}$ plot for reference samples (MPI-DING glasses and rutile R10). $\Delta_{Nb/Ta}$ = (measured Nb/Ta − published reference value)/published reference value. The ratio shows little systematic dependence on increasing Ti-content: a positive deviation of <5% (mostly <3%) for MPI-DING glasses, and ~9% for pure rutile (R10) when compared to Zack's data (unpublished), which are based on an average of two measurements.

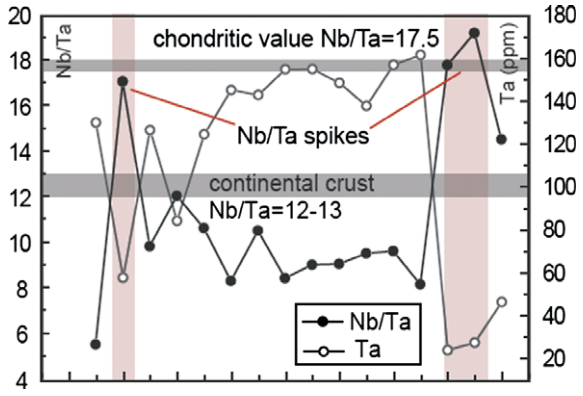

Fig. 5. Nb/Ta variations within a rutile grain (27a-1) from eclogite. Also shown are the Nb/Ta ratio for chondrites (McDonough and Sun, 1995) and for the CC (Barth et al., 2000). The cores of rutile grains have subchondritic Nb/Ta lower than that of the CC with high Nb, Ta contents. The Nb/Ta usually increases sharply to suprachondritic coupled with lower Nb, Ta contents near the rims, forming "Nb/Ta spikes." The Nb/Ta then drops quickly to subchondritic with high Nb and Ta. Thus, the Nb/Ta ratios can be separated into three groups: the cores and the rims with Nb/Ta spikes in between.

due to dehydration processes that occurred at shallower depths before rutile appears, or when rutile is unstable. These facts also imply that other Ti-minerals, e.g., titanite and ilmenite, have not been involved during the dehydration processes that mobilized Ti, Nb, Ta, and fractionated Nb/Ta, because of the high Ti, Nb, Ta concentrations in these minerals (Barth et al., 2002; Prowatke and Klemme, 2005).

Ti-minerals (mostly rutile, titanite, and sometime also ilmenite) have been reported from blueschists and eclogites (Chopin et al., 1991; Carswell et al., 1996; Liou et al., 1998; Gao et al., 1999; Tsujimori, 2002). Experiments with a tholeiitic basalt at temperatures of 600–950 °C show that titanite at low temperatures and ilmenite at high temperatures occur essentially at pressures <1.5 GPa (Liou et al., 1998), whereas rutile appears at pressures >1.5 GPa (Liou et al., 1998; Xiong et al., 2005). Interestingly, titanite and ilmenite in our samples are retrograde products of rutile, occurring as thin rims surrounding rutile grains or exsolutions (Fig. 2). No titanite inclusion in rutile grains has been identified. In fact, in blueschists and eclogites, titanite often appears as retrograde product of rutile (Carswell et al., 1996; Gao et al., 1999; Tsujimori, 2002). These facts indicate that rutile is likely to be the first Ti-mineral in many blueschists and eclogites, possibly because the subducting slab was not heated up to temperatures suitable for titanite formation before pressures reached 1.5 GPa. It has not been investigated experimentally yet at what temperature titanite starts to appear. Assuming the lowest temperature (600 °C) for the long-run-duration experiments (Liou et al., 1998) is the onset temperature of titanite formation, the dehydration that fractionated Nb/Ta should have occurred at pressures <1.5 GPa and temperatures <600 °C.

Dehydration has been proposed as the main mechanism that fractionates Nb from Ta (Ionov and Hofmann, 1995; Kamber and Collerson, 2000; Rapp et al., 2003) because element distributions in most magmatic processes are charge and radius controlled, and as such, the most efficient way of fractionating Nb from Ta is chemical complexing in hydrous solution. Such a simple dehydration model, however, has not been widely accepted: First, hydrous fluids usually have low Nb and Ta contents in the presence of rutile (Brenan et al., 1994; Stalder et al., 1998), and are therefore unlikely to be able to control the Nb, Ta budget of the subducting slabs. Second, if there is no rutile in the system, fluids equilibrated with clinopyroxene and garnet should have Nb/Ta considerably higher than the bulk rock (Stalder et al., 1998), which cannot explain the subchondritic Nb/Ta of the continental crust. Moreover, the Nb/Ta in modern arc rocks are usually not subchondritic (Eggins et al., 1997; Munker et al., 2004), indicating that simple dehydration is unlikely to be the sole process that contributed to the Nb/Ta fractionation. There must be additional processes that have selectively transferred subchondritic Nb/Ta to the continental crust. All these problems can be conceivably resolved by dehydration-induced Nb/Ta fractionation ± dehydration melting.

5.2. "Zone refining" dehydration model

Subducting slabs are not homogenous in terms of temperature and water contents at the early stage of subduction. In general, the temperature increases while the

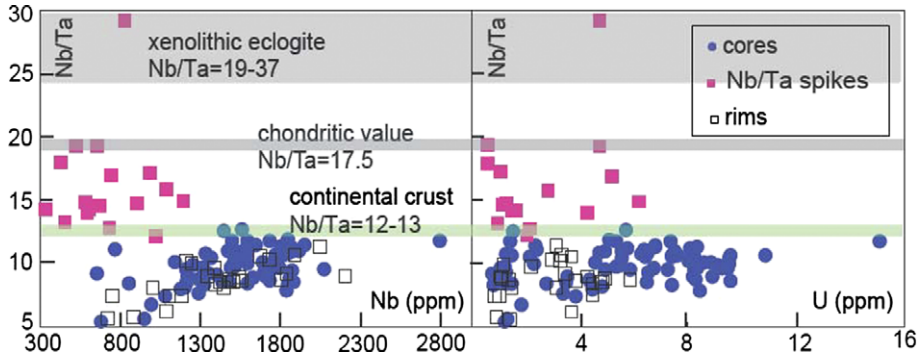

Fig. 6. Nb/Ta versus Nb and U for investigated rutile grains. Also shown are the Nb/Ta for chondrites (McDonough and Sun, 1995), the CC (Barth et al., 2000) and xenolithic eclogites (Rudnick et al., 2000). The cores and the rims are similar to each other, forming positive correlations, whereas the Nb/Ta spikes fall off the lines, with lower Nb and U contents, indicating that the Nb, Ta fractionation was controlled by at least two different processes (see text).

water content varies from the surface of the slab to the mantle lithosphere before subduction (Hacker et al., 2003). During subduction, the slab is heated up from both the bottom and the top. So, at the early stage of subduction, the subducting slab may have a "sandwich" structure, with colder regions bounded by hotter layers both on the slab surface and inside the slab. In the hotter parts of the slab, major dehydration occurs during blueschist to amphibole–eclogite transformation (BAT) that takes place in the absence of rutile (<1.5 GPa) (Fig. 7). In this case, Nb and Ta budgets are controlled by the partitioning between fluids and amphibole.

In a Ti-mineral-free system, amphibole has higher Nb, Ta compared to other minerals in rocks ranging from mantle peridotite (Witt-Eickschen and Harte, 1994; Ionov and Hofmann, 1995; Chazot et al., 1996) to syenites and granites (Marks et al., 2004). There are no partitioning data of amphibole versus fluid for Nb and Ta so far. Nonetheless, it has been demonstrated that amphibole prefers Nb over Ta compared to melt and clinopyroxene (Ionov and Hofmann, 1995; Foley et al., 2002). The lower the mg number in amphibole, the more it prefers Nb (Foley et al., 2002). The $D_{amphibole/CPX}$ for Nb is about 2.5 times higher than that for Ta, estimated for high mg amphibole from veins in mantle xenoliths (Ionov and Hofmann, 1995), and can be as high as 8 times for quartz syenite (Marks et al., 2004). The $D_{amphibole/CPX}$ ratio of Nb versus Ta in metabasaltic rocks should lie between 2.5 and 8. Fluids also prefer Nb to Ta compared with CPX, with $D_{fluids/CPX}$ for Nb slightly less than 2 times higher than that for Ta (Stalder et al., 1998). Therefore, amphibole prefers Nb over Ta compared with fluids. In other words, fluids in equilibrium with amphibole should have low Nb/Ta. This is supported by the fact that amphibole favors Nb over Ta in systems that have been affected by fluids (Ionov and Hofmann, 1995; Marks et al., 2004). Therefore, the BAT fractionates Nb from Ta, resulting in subchondritic and suprachondritic Nb/Ta in the released fluids and residual amphibole eclogites, respectively. Ti is also mobile before the appearance of rutile, whereas hydrous minerals, such as amphibole and lawsonite, are stable in cold regions. Therefore,

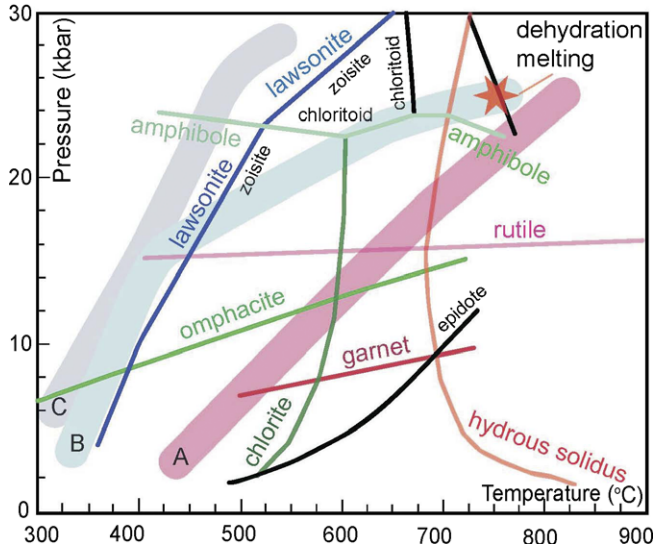

Fig. 7. Phase relations for subducting mid-ocean ridge basalts (modified after Schmidt and Poli, 1998 and Xiong et al., 2005) and different *P–T* regions (A–C) illustrating Nb/Ta fractionation in different portions of a subducting slab. Hot regions (A) inside a subducting slab are dehydrated at low pressures before rutile appears, releasing fluids with subchondritic Nb/Ta ratios. This portion of the slab will not melt during subduction because of its low water contents. In contrast, cold regions (B and C) in a subducting slab will not experience major dehydration before rutile appears and act as a sink of Nb, Ta and Ti in fluids released from the BAT in hot regions, which subsequently gathers fractionated Nb/Ta in rutile. In the Archean when the geotherm was high (B), hydrous eclogites were heated up relatively fast during further subduction, and were melted through dehydration-melting indicated by the star (Rapp et al., 2003; Rapp and Watson, 1995). For cold geotherm such as in modern convergent margins (C), hydrous eclogites will not be melted, but will be further dehydrated in the presence of rutile, without additional Nb/Ta fractionation.

hydrous fluids, together with trace and major elements (Nb, Ta, Ti, Si, etc.) released during the BAT in the hotter regions, are gradually transferred towards colder regions inside the subducting slab and subsequently retained by hydrous minerals. This is consistent with the observation that the investigated rutile-bearing hydrous eclogite layers are situated at depths between 40 and 500 m of the drill-

cores ZK703 and 300–600 m of the CCSD main hole (Zhang et al., 2004).

The mobility of Ti during early dehydration of the hotter regions leads to Ti depletion, which can result in rutile-free residual amphibole–eclogites even at high pressures in the dehydrated regions. In case there is no rutile, dehydration of these residual amphibole eclogites with suprachondritic Nb/Ta will further elevate the Nb/Ta in fluids, because both clinopyroxene and garnet favour Ta over Nb (Stalder et al., 1998). This can plausibly explain the Nb/Ta spikes of the rutile grains (Fig. 5). The low Nb/Ta ratios at the very margin were probably formed during retrograde metamorphism.

Such a ''zone refining'' dehydration process results in subchondritic Nb/Ta values in the colder and wetter regions, with complementary suprachondritic Nb/Ta in the hotter and dryer regions of the slabs. The dehydration induced Nb/Ta fractionation was probably even more efficient and more substantial in the early history of the Earth, as the oceanic crust was thicker with larger geothermal variations within subducting slabs (Rudnick et al., 2000).

In addition to dehydration of basaltic portions of the slab, dehydration of serpentinites is likely to be an important source of fluids (Hattori and Guillot, 2003). These fluids should have passed though the basaltic layer after being released, which might also fractionate Nb and Ta in case *P–T* conditions are favourable.

5.3. The fate of the fractionated Nb/Ta signature and the formation of the CC

For cold geotherms such as in modern subduction zones, amphibole breaks at pressures of ~2.5 GPa (Schmidt and Poli, 1998; Xiong et al., 2005), long after rutile appears (Liou et al., 1998; Xiong et al., 2005). No major slab melting occurs, except for the subduction of young hot oceanic crust, which produces adakite. Consequently, Ti, Nb, and Ta are all retained in rutile, and thus are not mobile during amphibole–eclogite to eclogite transformation. Therefore, the fractionated Nb/Ta features are preserved and descended to greater depths. As a result, the fractionated Nb/Ta signature cannot be systematically transferred to modern arc magmas. This explains the lack of systematic subchondritic Nb/Ta in many modern arc volcanic rocks (Munker et al., 2004).

The fractionated Nb/Ta ratios of the subducting slabs can be transferred to the CC through slab melting. As subduction continues, the temperature of the subducting slab increases and becomes more homogenous. At this stage melting of the subducting slab is mainly controlled by H_2O contents. In the Archean, when the geotherm was hot, large proportions of the colder and wetter regions would be melted through dehydration-melting when they were heated up with increasing depths (Fig. 7). This resulted in large quantities of TTG magmas with subchondritic Nb/Ta values, as well as depletions of Nb, Ta and heavy rare earth elements because of residual rutile and garnet, respectively. The residues of the dehydration-melting have even lower Nb/Ta values. In contrast, the dry regions (early dehydrated inner portions) of the slab with suprachondritic Nb/Ta ratios cannot be melted. Therefore, refractory residual eclogites have highly variable Nb/Ta from subchondritic to suprachondritic, with an overall suprachondritic average Nb/Ta as observed in xenolithic eclogites from kimberlite pipes (Rudnick et al., 2000), which is complementary to the continental crust.

Acknowledgments

YLX's research was supported by the German National Science Foundation (DFG, HO 375/22) and partly by the National Science Foundation of China (40472036). WDS was supported by the Natural Science Foundation of China (40525010), the Chinese Academy of Science and the Alexander von Humboldt Foundation. We dedicate this paper to Dr. Shen-su Sun, a great scientist, who initiated this study with stimulating discussions and constructive suggestions, and helped to shape the findings reported here before he passed away. Valuable comments by Alan Brandon, Balz Kamber, Carsten Münker, and an anonymous reviewer materially improved the original manuscript and are greatly appreciated.

Associate editor: Alan D. Brandon

References

Abbott, D.H., Drury, R., Mooney, W.D., 1997. Continents as lithological icebergs: the importance of buoyant lithospheric roots. *Earth Planet. Sci. Lett.* **149** (1–4), 15–27.

Barth, M.G., McDonough, W.F., Rudnick, R.L., 2000. Tracking the budget of Nb and Ta in the continental crust. *Chem. Geol.* **165** (3–4), 197–213.

Barth, M.G., Rudnick, R.L., Horn, I., McDonough, W.F., Spicuzza, M.J., Valley, J.W., Haggerty, S.E., 2002. Geochemistry of xenolithic eclogites from West Africa, part 2: origins of the high MgO eclogites. *Geochim. Cosmochim. Acta* **66** (24), 4325–4345.

Brenan, J.M., Shaw, H.F., Phinney, D.L., Ryerson, F.J., 1994. Rutile-aqueous fluid partitioning of Nb, Ta, Hf, Zr, U and Th—implications for high-field strength element depletions in island-arc basalts. *Earth Planet. Sci. Lett.* **128** (3–4), 327–339.

Carswell, D.A., Wilson, R.N., Zhai, M., 1996. Ultra-high pressure aluminous titanites in carbonate-bearing eclogites at Shuanghe in Dabieshan, central China. *Mineral. Mag.* **60** (400), 461–471.

Carswell, D.A., Wilson, R.N., Zhai, M., 2000. Metamorphic evolution, mineral chemistry and thermobarometry of schists and orthogneisses hosting ultra-high pressure eclogites in the Dabieshan of central China. *Lithos* **52** (1–4), 121–155.

Chazot, G., Menzies, M.A., Harte, B., 1996. Determination of partition coefficients between apatite, clinopyroxene, amphibole, and melt in natural spinel lherzolites from Yemen: implications for wet melting of the lithospheric mantle. *Geochim. Cosmochim. Acta* **60** (3), 423–437.

Chopin, C., Henry, C., Michard, A., 1991. Geology and petrology of the coesite-bearing terrain, Dora-Maira Massif, Western Alps. *Eur. J. Miner.* **3** (2), 263–291.

Collins, W.J., 2002. Hot orogens, tectonic switching, and creation of continental crust. *Geology* **30** (6), 535–538.

Eggins, S.M., Woodhead, J.D., Kinsley, L.P.J., Mortimer, G.E., Sylvester, P., McCulloch, M.T., Hergt, J.M., Handler, M.R., 1997. A simple method for the precise determination of ⩾40 trace elements in geological samples by ICPMS using enriched isotope internal standardisation. *Chem. Geol.* **134** (4), 311–326.

Foley, S., Tiepolo, M., Vannucci, R., 2002. Growth of early continental crust controlled by melting of amphibolite in subduction zones. *Nature* **417** (6891), 837–840.

Foley, S.F., Barth, M.G., Jenner, G.A., 2000. Rutile/melt partition coefficients for trace elements and an assessment of the influence of rutile on the trace element characteristics of subduction zone magmas. *Geochim. Cosmochim. Acta* **64** (5), 933–938.

Fu, B., Touret, J.L.R., Zheng, Y.F., 2001. Fluid inclusions in coesite-bearing eclogites and jadeite quartzite at Shuanghe, Dabie Shan (China). *J. Metamorph. Geol.* **19** (5), 529–545.

Gao, J., Klemd, R., Zhang, L., Wang, Z., Xiao, X., 1999. *P–T* path of high-pressure/low-temperature rocks and tectonic implications in the western Tianshan Mountains, NW China. *J. Metamorph. Geol.* **17** (6), 621–636.

Gao, S., Rudnick, R.L., Yuan, H.L., Liu, X.M., Liu, Y.S., Xu, W.L., Ling, W.L., Ayers, J., Wang, X.C., Wang, Q.H., 2004. Recycling lower continental crust in the North China craton. *Nature* **432** (7019), 892–897.

Hacker, B.R., Abers, G.A., Peacock, S.M., 2003. Subduction factory-1. Theoretical mineralogy, densities, seismic wave speeds, and H_2O contents. *J. Geophys. Res. Solid Earth* **108** (B1). doi:10.1029/2001JB00112.

Hartmann, G., 1994. Late-medieval glass manufacture in the Eichsfeld Region (Thuringia, Germany). *Chem. der Erde* **54**, 103–128.

Hattori, K.H., Guillot, S., 2003. Volcanic fronts form as a consequence of serpentinite dehydration in the forearc mantle wedge. *Geology* **31** (6), 525–528.

Henry, C., Burkhard, M., Goffe, B., 1996. Evolution of synmetamorphic veins and their wallrocks through a western Alps transect: No evidence for large-scale fluid flow. Stable isotope, major- and trace-element systematics. *Chem. Geol.* **127** (1–3), 81–109.

Ionov, D.A., Hofmann, A.W., 1995. Nb–Ta-rich mantle amphiboles and micas—implications for subduction-related metasomatic trace-element fractionations. *Earth Planet. Sci. Lett.* **131** (3–4), 341–356.

Jochum, K.P., Dingwell, D.B., Rocholl, A., Stoll, B., Hofmann, A.W., Becker, S., Besmehn, A., Bessette, D., Dietze, H.J., Dulski, P., Erzinger, J., Hellebrand, E., Hoppe, P., Horn, I., Janssens, K., Jenner, G.A., Klein, M., McDonough, W.F., Maetz, M., Mezger, K., Munker, C., Nikogosian, I.K., Pickhardt, C., Raczek, I., Rhede, D., Seufert, H.M., Simakin, S.G., Sobolev, A.V., Spettel, B., Straub, S., Vincze, L., Wallianos, A., Weckwerth, G., Weyer, S., Wolf, D., Zimmer, M., 2000. The preparation and preliminary characterisation of eight geological MPI-DING reference glasses for in-site microanalysis. *Geostandards Newsl. J. Geostandards Geoanal.* **24** (1), 87–133.

Jochum, K.P., McDonough, W.F., Palme, H., Spettel, B., 1989. Compositional constraints on the continental lithospheric mantle from trace elements in spinel peridotite xenoliths. *Nature* **340**, 548.

Jochum, K.P., Seufert, H.M., Spettel, B., Palme, H., 1986. The solar system abundances of Nb, Ta and Y and the relative abundances of refractory lithophile elements in differentiated planetary bodies. *Geochim. Cosmochim. Acta* **50**, 1173–1183.

Kamber, B.S., Collerson, K.D., 2000. Role of 'hidden' deeply subducted slabs in mantle depletion. *Chem. Geol.* **166** (3–4), 241–254.

Kamber, B.S., Ewart, A., Collerson, K.D., Bruce, M.C., McDonald, G.D., 2002. Fluid-mobile trace element constraints on the role of slab melting and implications for Archaean crustal growth models. *Contrib. Mineral. Petrol.* **144** (1), 38–56.

Klemme, S., Prowatke, S., Hametner, K., Gunther, D., 2005. Partitioning of trace elements between rutile and silicate melts: implications for subduction zones. *Geochim. Cosmochim. Acta* **69** (9), 2361–2371.

Li, S., Jagoutz, E., Chen, Y., Li, Q., 2000. Sm–Nd and Rb–Sr isotopic chronology and cooling history of ultrahigh pressure metamorphic rocks and their country rocks at Shuanghe in the Dabie Mountains, central China. *Geochim. Cosmochim. Acta* **64** (6), 1077–1093.

Li, S., Wang, S., Chen, Y., Liu, D., Ji, Q., Zhou, H., Zhang, Z., 1994. Excess argon in phengite from eclogite: evidence from dating of eclogite minerals by Sm–Nd, Rb–Sr and $^{40}Ar/^{39}Ar$ methods. *Chem. Geol.* **112** (3–4), 343–350.

Li, S., Xiao, Y., Liou, D., Chen, Y., Ge, N., Zhang, Z., Sun, S.-s., Cong, B., Zhang, R., Hart, S.R., Wang, S., 1993. Collision of the North China and Yangtse blocks and formation of coesite-bearing eclogites: timing and processes. *Chem. Geol.* **109** (1–4), 89–111.

Li, X.H., Li, Z.X., Zhou, H.W., Liu, Y., Kinny, P.D., 2002. U–Pb zircon geochronology, geochemistry and Nd isotopic study of Neoproterozoic bimodal volcanic rocks in the Kangdian Rift of South China: implications for the initial rifting of Rodinia. *Precambrian Res.* **113** (1–2), 135–154.

Liou, J.G., Zhang, R.Y., 1995. Significance of ultrahigh-P talc-bearing eclogitic assemblages. *Mineral. Mag.* **59** (394), 93–102.

Liou, J.G., Zhang, R.Y., Ernst, W.G., Liu, J., McLimans, R., 1998. Mineral parageneses in the Piampaludo eclogitic body, Gruppo di Voltri, Western Ligurian Alps. *Schweiz. Mineral. Petrograph. Mitteilungen* **78** (2), 317–335.

Liou, J.G., Zhang, R.Y., Jahn, B.M., 2000. Petrological and geochemical characteristics of ultrahigh-pressure metamorphic rocks from the Dabie-Sulu terrane, east-central China. *Int. Geol. Rev.* **42** (4), 328–352.

Marks, M., Halama, R., Wenzel, T., Markl, G., 2004. Trace element variations in clinopyroxene and amphibole from alkaline to peralkaline syenites and granites: implications for mineral-melt trace-element partitioning. *Chem. Geol.* **211** (3–4), 185–215.

Martin, H., 1999. Adakitic magmas: modern analogues of Archaean granitoids. *Lithos* **46** (3), 411–429.

McDonough, W.F., 1991. Partial melting of subducted oceanic-crust and isolation of its residual eclogitic lithology. *Philos. Trans. R. Soc. Lond. Math. Phys. Eng. Sci.* **335** (1638), 407–418.

McDonough, W.F., Sun, S.S., 1995. The composition of the Earth. *Chem. Geol.* **120** (3–4), 223–253.

Munker, C., Pfander, J.A., Weyer, S., Buchl, A., Kleine, T., Mezger, K., 2003. Evolution of planetary cores and the earth-moon system from Nb/Ta systematics. *Science* **301** (5629), 84–87.

Munker, C., Worner, G., Yogodzinski, G., Churikova, T., 2004. Behaviour of high field strength elements in subduction zones: constraints from Kamchatka–Aleutian arc lavas. *Earth Planet. Sci. Lett.* **224** (3–4), 275–293.

Niu, Y.L., Batiza, R., 1997. Trace element evidence from seamounts for recycled oceanic crust in the eastern Pacific mantle. *Earth Planet. Sci. Lett.* **148** (3–4), 471–483.

Okay, A.I., 1995. Paragonite eclogites from Dabie-Shan, China—re-equilibration during exhumation. *J. Metamorph. Geol.* **13** (4), 449–460.

Pearce, J.A., Peate, D.W., 1995. Tectonic implications of the composition of volcanic arc magmas. *Annu. Rev. Earth Planet. Sci.* **23**, 251–285.

Plank, T., Langmuir, C.H., 1998. The chemical composition of subducting sediment and its consequences for the crust and mantle. *Chem. Geol.* **145** (3–4), 325–394.

Prowatke, S., Klemme, S., 2005. Effect of melt composition on the partitioning of trace elements between titanite and silicate melt. *Geochim. Cosmochim. Acta* **69** (3), 695–709.

Rapp, R.P., Shimizu, N., Norman, M.D., 2003. Growth of early continental crust by partial melting of eclogite. *Nature* **425** (6958), 605–609.

Rapp, R.P., Watson, E.B., 1995. Dehydration melting of metabasalt at 8–32 kbar—implications for continental growth and crust-mantle recycling. *J. Petrol.* **36** (4), 891–931.

Reynaud, C., Jaillard, E., Lapierre, H., Mamberti, M., Mascle, G.H., 1999. Oceanic plateau and island arcs of southwestern Ecuador: their place in the geodynamic evolution of northwestern South America. *Tectonophysics* **307** (3–4), 235–254.

Rudnick, R.L., 1995. Making continental-crust. *Nature* **378** (6557), 571–578.

Rudnick, R.L., Barth, M., Horn, I., McDonough, W.F., 2000. Rutile-bearing refractory eclogites: missing link between continents and depleted mantle. *Science* **287** (5451), 278–281.

Rudnick, R.L., Fountain, D.M., 1995. Nature and composition of the continental-crust—a lower crustal perspective. *Rev. Geophys.* **33** (3), 267–309.

Schmidt, M.W., Dardon, A., Chazot, G., Vannucci, R., 2004. The dependence of Nb and Ta rutile-melt partitioning on melt composition and Nb/Ta fractionation during subduction processes. *Earth Planet. Sci. Lett.* **226** (3–4), 415–432.

Schmidt, M.W., Poli, S., 1998. Experimentally based water budgets for dehydrating slabs and consequences for arc magma generation. *Earth Planet. Sci. Lett.* **163**, 361–379.

Shannon, R.D., 1976. Revised effective ionic-radii and systematic studies of interatomic distances in halides and chalcogenides. *Acta Crystallographica Section A* **32**(SEP1), 751–767.

Smithies, R.H., 2000. The Archaean tonalite–trondhjemite–granodiorite (TTG) series is not an analogue of Cenozoic adakite. *Earth Planet. Sci. Lett.* **182** (1), 115–125.

Spandler, C., Hermann, J., Arculus, R., Mavrogenes, J., 2003. Redistribution of trace elements during prograde metamorphism from lawsonite blueschist to eclogite facies, implications for deep subduction-zone processes. *Contrib. Mineral. Petrol.* **146** (2), 205–222.

Stalder, R., Foley, S.F., Brey, G.P., Horn, I., 1998. Mineral aqueous fluid partitioning of trace elements at 900–1200 degrees C and 3.0–5.7 GPa: new experimental data for garnet, clinopyroxene, and rutile, and implications for mantle metasomatism. *Geochim. Cosmochim. Acta* **62** (10), 1781–1801.

Sun, S.S., McDonough, W.F., 1989. Chemical and isotopic systematics of oceanic basalts; implications for mantle composition and processes. In: Saunders, A.D., Norry, M.J. (Eds.), *Magmatism in the Ocean Basins*, vol. 42. Geological Society of London, pp. 313–345.

Sun, W., Bennett, V.C., Eggins, S.M., Arculus, R.J., Perfit, M.R., 2003. Rhenium systematics in submarine MORB and back-arc basin glasses: laser ablation ICP-MS results. *Chem. Geol.* **196** (1–4), 259–281.

Sun, W.D., 2003. *The Subduction Factory, a Perspective from Rhenium and Trace Element Geochemistry of Oceanic Basalts and Eclogites*. Ph.D. Thesis, Australian National University.

Sun, W.D., Williams, I.S., Li, S.G., 2002. Carboniferous and Triassic eclogites in the western Dabie Mountians, east-central China: evidence for protracted convergence of the North and South China Blocks. *J. Metamorph. Geol.* **20**, 873–886.

Taylor, S.R., McLennan, S.M., 1985. *The Continental Crust: Its Composition and Evolution*. Blackwell, Oxford.

Tsujimori, T., 2002. Prograde and retrograde *P–T* paths of the late Paleozoic glaucophane eclogite from the Renge metamorphic belt, Hida Mountains, southwestern Japan. *Int. Geol. Rev.* **44** (9), 797–818.

Weyer, S., Munker, C., Mezger, K., 2003. Nb/Ta, Zr/Hf and REE in the depleted mantle: implications for the differentiation history of the crust-mantle system. *Earth Planet. Sci. Lett.* **205** (3–4), 309–324.

Witt-Eickschen, G., Harte, B., 1994. Distribution of trace-elements between amphibole and clinopyroxene from mantle peridotites of the Eifel (Western Germany)—an ion-microprobe study. *Chem. Geol.* **117** (1–4), 235–250.

Xiao, Y.L., Hoefs, J., Kronz, A., 2005. Compositionally zoned Cl-rich amphiboles from North Dabie Shan, China: Monitor of high-pressure metamorphic fluid/rock interaction processes. *Lithos* **81** (1–4), 279–295.

Xiao, Y.L., Hoefs, J., van den Kerkhof, A.M., Fiebig, J., Zheng, Y., 2000. Fluid history of UHP metamorphism in Dabie Shan, China; a fluid inclusion and oxygen isotope study on the coesite-bearing eclogite from Bixiling. *Contrib. Miner. Petrol.* **139** (1), 1–16.

Xiao, Y.L., Hoefs, J., van den Kerkhof, A.M., Simon, K., Fiebig, J., Zheng, Y.F., 2002. Fluid evolution during HP and UHP metamorphism in Dabie Shan, China: constraints from mineral chemistry, fluid inclusions and stable isotopes. *J. Petrol.* **43** (8), 1505–1527.

Xiong, X.L., Adam, J., Green, T.H., 2005. Rutile stability and rutile/melt HFSE partitioning during partial melting of hydrous basalt: implication for TTG genesis. *Chem. Geol.* **218** (3–4), 339–359.

Xu, S., Okay, A.I., Ji, S., Sengor, A.M.C., Su, W., Liu, Y., Jiang, L., 1992. Diamond from the Dabie Shan metamorphic rocks and its implication for tectonic setting. *Science* **256** (5053), 80–82.

Xu, Z.Q., 2004. The scientific goals and investigation progresses of the Chinese Continental Scientific Drilling Project. *Acta Petrol. Sin.* **20** (1), 1–8.

Xu, Z.Q., Yang, W.C., Zhang, Z.M., Yang, T.N., 1998. Scientific significance and site-selection researches of the first Chinese Continental Scientific Deep Drillhole. *Cont. Dyn.* **3**, 1–13.

Yang, J.J., Jahn, B.M., 2000. Deep subduction of mantle-derived garnet peridotites from the Su–Lu UHP metamorphic terrane in China. *J. Metamorph. Geol.* **18** (2), 167–180.

Yui, T.F., Rumble, D., Lo, C.H., 1995. Unusually low delta-O-18 ultrahigh-pressure metamorphic rocks from the Sulu Terrain, Eastern China. *Geochim. Cosmochim. Acta* **59** (13), 2859–2864.

Zack, T., Kronz, A., Foley, S.F., Rivers, T., 2002. Trace element abundances in rutiles from eclogites and associated garnet mica schists. *Chem. Geol.* **184** (1–2), 97–122.

Zack, T., von Eynatten, H., Kronz, A., 2004. Rutile geochemistry and its potential use in quantitative provenance studies. *Sediment. Geol.* **171** (1–4), 37–58.

Zhang, R.Y., Hirajima, T., Banno, S., Cong, B., Liou, J.G., 1995. Petrology of ultrahigh-pressure rocks from the southern Su–Lu region, eastern China. *J. Metamorph. Geol.* **13** (6), 659–675.

Zhang, Z.M., Xu, Z.Q., Liu, F.L., You, Z.D., Shen, K., Yang, J.S., Li, T.F., Chen, C.Z., 2004. Geochemistry of eclogites from the main hole (100 to 2050 m) of the Chinese Continental Scientific Drilling Project. *Acta Petrol. Sin.* **20** (1), 27–42.

Zhao, R.X., Liou, J.G., Zhang, R.Y., Wooden, J.L., 2005. SHRIMP U–Pb dating of zircon from the Xugou UHP eclogite, Sulu terrane, eastern China. *Int. Geol. Rev.* **47** (8), 805–814.

Zheng, Y.F., Fu, B., Gong, B., Li, L., 2003. Stable isotope geochemistry of ultrahigh pressure metamorphic rocks from the Dabie-Sulu orogen in China: implications for geodynamics and fluid regime. *Earth Sci. Rev.* **62** (1–2), 105–161.

Zheng, Y.F., Fu, B., Li, Y.L., Xiao, Y.L., Li, S.G., 1998. Oxygen and hydrogen isotope geochemistry of ultrahigh-pressure eclogites from the Dabie Mountains and the Sulu terrane. *Earth Planet. Sci. Lett.* **155** (1–2), 113–129.